Earth and Planetary Science Letters 576 (2021) 117198

Contents lists available at ScienceDirect

Earth and Planetary Science Letters

www.elsevier.com/locate/epsl

Rapid pre-eruptive mush reorganisation and atmospheric volatile emissions from the 12.9 ka Laacher See eruption, determined using apatite

M.C.S. Humphreys[a,*], V.C. Smith[b], J.P. Coumans[a,1], J.M. Riker[a,d], M.J. Stock[c,e], J.C.M. de Hoog[f], R.A. Brooker[d]

[a] *Department of Earth Sciences, Durham University, Science Labs, Stockton Road, Durham, DH1 3LE, UK*
[b] *RLAHA, University of Oxford, UK*
[c] *Department of Earth Sciences, University of Oxford, South Parks Road, Oxford, OX1 3AN, UK*
[d] *School of Earth Sciences, University of Bristol, UK*
[e] *Department of Geology, Trinity College Dublin, University of Dublin, Dublin 2, Ireland*
[f] *School of Geosciences, University of Edinburgh, UK*

ARTICLE INFO

Article history:
Received 2 September 2020
Received in revised form 25 August 2021
Accepted 5 September 2021
Available online 12 October 2021
Editor: C.M. Petrone

Keywords:
apatite
volatiles
crystal mush
magma eruptibility
Laacher See
halogens

ABSTRACT

Magma is commonly thought to be stored as a crystal-rich mush within vertically extensive, crustal storage regions. A key unknown is how to remobilise and erupt such crystal-rich material, and whether the growth of gas bubbles within the mush could promote remobilisation. In order to investigate this, we need improved constraints on the timing of volatile saturation in magmas. The mineral apatite represents a potentially useful record of pre-eruptive magmatic volatiles, but data interpretation is complex because exchange reactions control the volatile partitioning. Model solutions are therefore non-unique. Here, we present a numerical forward modelling program with a sensitivity analysis function, which addresses non-uniqueness by identifying alternative sets of starting parameters that match a target compositional trend through a population of apatite crystals. The model is applied to a new dataset of volatiles in apatite from the 12.9 ka Laacher See eruption, Eifel volcanic region, Germany. The results indicate that the magma was initially strongly volatile-undersaturated and became saturated through progressive crystal fractionation. Apatite crystals are not in volatile or trace element equilibrium with their carrier melts, indicating dispersal of crystals into different chemical environments. Consideration of apatite diffusivities suggests that this reorganisation occurred shortly before eruption. Our modelling results also allow us to constrain directly the amount of pre-eruptive magmatic vapour emitted during the explosive eruption, highlighting the importance of considering the behaviour of halogens during magma storage. Overall, our approach confirms the value of measuring apatite volatile contents and highlights the potential of this method to provide quantitative constraints on magmatic evolution and storage conditions.

1. Introduction

Dissolved volatiles (H_2O, S, CO_2, halogens) are important constituents of magmas at depth within the Earth's crust. Volatiles affect phase relationships as well as physical properties such as melt and magma viscosity and density. When a magma becomes volatile saturated, the presence of exsolved fluid can drastically change the bulk magma density and cause pressure to build up within the magma storage region. Exsolution of volatiles and bubble expansion during magma ascent are a key driver for explosive volcanic activity at the surface (e.g. Sparks, 1978), but bubble growth during magma storage could also contribute to explosive volcanism through unjamming and remobilisation of cool, otherwise uneruptible crystal-rich mushes (e.g. Truby, 2016). Understanding the significance of these processes is important because such potentially eruptible crystal mushes may be undetected by geophysical observations (Cashman et al., 2017), which means that associated hazards could remain unidentified. However, more information is first needed about the timing and depth of volatile saturation in magmatic systems. Melt inclusions are commonly used to measure pre-eruptive dissolved volatile concentrations, but the inclusions can be significantly compromised by diffusive volatile migration, as

---

[*] Corresponding author.
E-mail address: madeleine.humphreys@durham.ac.uk (M.C.S. Humphreys).
[1] Present address: CanmetMINING, Natural Resources Canada, Canada.

https://doi.org/10.1016/j.epsl.2021.117198

well as by decrepitation or post-entrapment crystallisation of the host mineral. In particular, volatiles can diffuse into shrinkage bubbles within the inclusions (Moore et al., 2015), or through the host mineral, particularly during slower magma ascent (e.g. Portnyagin et al., 2008). Thus, measurements of dissolved volatile concentrations in melt inclusions can be an unreliable record of pre-eruptive magmatic volatile abundances.

An alternative record of pre-eruptive melt volatile compositions is available through the accessory mineral apatite, $Ca_5(PO_4)_3$-(OH,F,Cl), which incorporates volatiles directly into its crystal structure. The hexagonal channel site, which runs parallel to the crystallographic c-axis, is occupied primarily by OH+F+Cl, and a series of exchange equilibria link the volatile compositions of the apatite to those of the melt (Candela, 1986). Apatite can therefore be used to interpret magmatic volatile contents (e.g. Boyce and Hervig, 2008; Candela, 1986; Douce et al., 2011; Li and Costa, 2020; Popa et al., 2021), to understand the timing of volatile saturation (Candela, 1986; Stock et al., 2018, 2016), and to bring new constraints on the compositions of fluids in magmatic-hydrothermal settings (e.g. Boudreau and McCallum, 1989; Brenan, 1993; Candela and Holland, 1986; Doherty et al., 2014). However, a key challenge in exploiting this potential is that the volatiles compete to fill a stoichiometric crystal site through exchange reactions, rather than through a simple Henrian partition coefficient. For example, F-rich apatite could equally result from either F-enrichment or OH (±Cl) depletion in the melt, as well as from decreasing temperature (e.g. Boyce et al., 2014; Brenan, 1993; Riker et al., 2018). This means that interpretations of the equilibrium melt volatile contents are non-unique. Here, we address this problem directly through a quantitative numerical model (based on Stock et al., 2018) that describes the variation of apatite OH-F-Cl compositions during fractionation, but, crucially, can also be used to examine the sensitivity of model results to individual parameters, and explore the range of conditions that can reproduce compositional trends observed in natural or experimental datasets.

We apply the model to apatites from the Laacher See Tephra (Germany) and show that portions of the magmatic system were initially volatile-undersaturated, but evolved towards volatile saturation during fractionation. Apatite crystals are not in volatile equilibrium with their carrier melts. This lack of equilibrium indicates that crystals must have been dispersed into different melts before eruption. Combined with the high diffusivities of volatiles in apatite, these results indicate that eruption was immediately preceded by structural reorganisation of an extensive, crystal-rich mush. In addition, the modelling allows us to estimate the atmospheric mass loading of both halogens and H_2O during the eruption, bringing new constraints on the atmospheric impact of this large, explosive eruption.

2. The model framework

The behaviour of volatiles in igneous apatite during silicate melt crystallisation was first described by Candela (1986) for both vapour-saturated and undersaturated conditions, assuming ideal mixing in the apatite volatile site. In that model, the halogens were treated as perfectly incompatible. X_{OH} was calculated by mass balance, although this introduces uncertainties due to the presence of other species such as CO_3^{2-} and the formation of oxyapatite (Riker et al., 2018), as well as uncertainties resulting from complex stoichiometry calculations. The Candela (1986) model predicted qualitative trends for apatite volatile composition, but tended to perform poorly for fluorine (e.g. Riker et al., 2018). Douce et al. (2011) also calculated apatite X_{OH} by mass balance using a quasi-chemical approach that includes the effects of changing Ca activity and phosphate content, but their model considered only apatite, melt and fluid as possible reservoirs for volatiles, neglecting other potentially important crystal hosts. Furthermore, the model did not accommodate Cl-OH exchange between fluid and melt, which is particularly important in intermediate and alkaline rocks where $D_{Cl}^{fl-m} \gg 1$ and $D_{F}^{fl-m} \sim 1$ (Webster et al., 2009). Stock et al. (2018) modelled the evolving compositions of apatites formed during fractional crystallisation ± degassing, based on Candela (1986) but incorporating non-zero crystal-melt partition coefficients for volatiles, and explicit prediction of all three volatile species. Popa et al. (2021) used a similar approach to model apatite compositions in the Aegean. Finally, Li and Costa (2020) presented a thermodynamic model that incorporates non-ideal mixing on the volatile site and can accommodate direct measurement of X_{OH}^{ap}. This approach takes the measured apatite volatile composition and uses information about the magma temperature and halogen contents to calculate exchange coefficients, and thus to infer the H_2O concentration of the host melt from either melt F or Cl contents (assuming equilibrium conditions). However, as with any mineral system, we would ultimately like to model populations of crystals and take into account complex processes involving both melt, anhydrous and/or volatile-bearing crystals, and fluid components, while also understanding the range of possible conditions that could match the measured apatite compositions.

In order to do this, we build on the model of Stock et al. (2018), by implementing in MATLAB a forward modelling approach to track the behaviour of Cl, F and OH in apatite, melt and fluid during fractional crystallisation and volatile exsolution, and to assess the sensitivity of results to alternative inputs. As in Stock et al. (2018), the volatile composition of apatite is described using a series of apatite-melt exchange equilibria, such as:

$$Ca_5(PO_4)_3Cl_{ap} + OH_m = Ca_5(PO_4)_3OH_{ap} + Cl_m \tag{1}$$

otherwise expressed in mole fraction terms as:

$$X_{Cl}^{ap} + X_{OH}^{m} = X_{OH}^{ap} + X_{Cl}^{m} \text{ etc.,} \tag{2}$$

where X_i^j is the mole fraction of component i in phase j. For simplicity, we assume that the typically small amounts of carbonate measured in apatite (Riker et al., 2018; Stock et al., 2016) do not affect the mole fraction calculations. We also assume ideal mixing of OH-F-Cl in apatite, fluid and melt (for a discussion, see later). Each element (F, Cl and water) is assigned a (fixed) bulk crystal-melt partition coefficient (D_i^{xl-m}) and a bulk fluid-melt partition coefficient (D_i^{fl-m}). The use of fixed bulk D_i^{xl-m} differs from the approach of Boyce et al. (2014) and McCubbin et al. (2016) but is well justified for hydrous, halogen-rich systems such as the Laacher See, where apatite (together with other volatile-bearing phases) crystallises early. Other model input parameters include the initial melt volatile contents $C_{0,i}^{m}$ (where i is Cl, F and water) and exchange coefficients (K_D) that describe the exchange reactions for the apatite volatile site, $K_{\text{Cl-OH}}$, $K_{\text{F-OH}}$ and $K_{\text{F-Cl}}$, e.g.:

$$K_{Cl-OH}^{ap-m} = \frac{a_{Cl}^{ap}}{a_{OH}^{ap}} \cdot \frac{a_{OH}^{m}}{a_{Cl}^{m}} \tag{3}$$

This gives a system of equations to link the ternary volatile components in apatite with melt composition and K_D, following Candela (1986):

$$X_{Cl}^{ap} = 1 \Bigg/ \left[1 + \frac{X_F^m}{X_{Cl}^m \cdot K_{Cl-F}^{ap-m}} + \frac{X_{OH}^m}{X_{Cl}^m \cdot K_{Cl-OH}^{ap-m}} \right] \tag{4}$$

$$X_{F}^{ap} = 1 \Bigg/ \left[1 + \frac{K_{Cl-F}^{ap-m} \cdot X_{Cl}^m}{X_F^m} + \frac{X_{OH}^m}{X_F^m \cdot K_{F-OH}^{ap-m}} \right] \tag{5}$$

$$X_{OH}^{ap} = 1 / \left[1 + \frac{X_{Cl}^{m} \cdot K_{Cl-OH}^{ap-m}}{X_{OH}^{m}} + \frac{X_{F}^{m} \cdot K_{F-OH}^{ap-m}}{X_{OH}^{m}} \right] \tag{6}$$

For each increment of bulk crystal fractionation, we first calculate the evolution of F, Cl and H_2O in the melt ± fluid:

$$C_i^m = C_0^m \cdot F^{\left(D_i^{xl-m} - 1\right)} \tag{7}$$

We account for fluid saturation when the evolving melt H_2O content reaches its pre-defined solubility limit by calculating the amount of fluid exsolved at each increment (j) of fractionation:

$$\text{wt\% } H_2O^{fl} = C_{H_2O}^{0} \cdot F^{(D-1)} - C_{H_2O}^{sat} \tag{8}$$

The halogen concentration of this fluid is then calculated through the fluid-melt partition coefficient, following Candela and Holland (1986), e.g.:

$$\text{wt\% } Cl^{fl} = C_{Cl}^{m} \cdot D_{Cl}^{fl-m} = Cl_m^{j-1} \left(\frac{F^j}{F^{j-1}} \right)^{\left(D_{Cl}^{xl-m} - 1\right)} \tag{9}$$

Finally, we use mass balance to compute the concentration of halogens remaining in the melt following that fractionation step, by:

$$\text{wt\% } Cl^{m} = C_{Cl}^{m} - Cl^{fl} \cdot H_2O^{fl} \tag{10}$$

where C_{Cl}^{m} is from (7), C_{Cl}^{fl} is from (9) and H_2O^{fl} is from (8). The mole fraction of volatile components in the melt is calculated following Li and Hermann (2015) and the speciation of water in the melt is calculated using the temperature-dependent equation of Zhang (1999).

The ternary components X_{OH}^{ap}, X_{F}^{ap} and X_{Cl}^{ap} of the equilibrium apatite are determined independently using Equations (4)-(6), and the stoichiometry of the modelled apatite volatile site can therefore be calculated as a measure of the internal consistency of the model results. Temperature is not explicitly included, although both the apatite-melt exchange coefficients, and the melt OH-H_2O equilibrium coefficient, are somewhat temperature dependent (Li and Costa, 2020; Riker et al., 2018; Zhang, 1999). To summarise: we first forward-model the volatile evolution of the melt, taking into account crystallisation of volatile-bearing mineral phases and separation of fluid. We then compute the compositions of apatite that would be in equilibrium with those melts at each stage of fractionation. The program is implemented in MATLAB and is provided as part of the Supplementary Information, together with comprehensive documentation, a user manual and a test dataset.

As outlined above, a significant challenge in using apatite to understand igneous processes is the competition for space in the apatite volatile site, which results in significant non-uniqueness in the compositions of calculated equilibrium melt and apatite (Boyce et al., 2014; Li and Costa, 2020; Stock et al., 2016). To address this, the program also includes an operation using the `multistart` global optimisation solver in MATLAB. This operation can be used to perform sensitivity analysis based on defined 'target' compositional trends. The basic forward model is run many times from randomly generated starting points, selected from within user-defined upper and lower bounds for every input parameter, generating a large family of predicted apatite compositional trends. Each resulting trend is evaluated against the target curve by calculating the root-mean-square error (RMSE), and only model results that match the target curve within a user-specified tolerance are returned (see Supplementary Information). The program can also be used to visualise these results by generating figures showing (i) all successful model runs, coloured by RMSE; (ii) histograms of input parameter values for all successful runs; and (iii) co-variations of input parameter values with RMSE in the successful runs.

3. Samples and analytical methods

The Laacher See Tephra (12.9 cal. ka BP) was erupted from the Eifel volcanic field, Germany, and is thought to represent material ejected from a continuously zoned magma column generated through crystal fractionation and mixing (Wörner and Schmincke, 1984a). The stratigraphy comprises the Lower (LLST), Middle (MLST) and Upper Laacher See Tephra (ULST). The LLST is a highly evolved, crystal-poor phonolite, interpreted to comprise the volatile-rich, evolved cap of a fractionating magma column (Wörner and Schmincke, 1984b). The MLST is a chemically zoned phonolite that becomes more primitive, and more crystal-rich upwards in the stratigraphy. The ULST is a crystal-rich, mafic phonolite that is mingled with basanite (Tomlinson et al., 2020; Wörner and Wright, 1984). The melt of the ULST is thought to be parental to the MLST and LLST, which are interpreted to have segregated from the crystallising mush zone and pooled at higher levels (Tomlinson et al., 2020; Wörner and Schmincke, 1984a). Tomlinson et al. (2020) showed that the melt phase contains abrupt compositional steps, indicating the presence of discrete melt lenses rather than a continuous compositional trend. The Laacher See Tephra is also strongly variable in modal mineralogy. Sanidine is abundant throughout the sequence but the ULST is enriched in clinopyroxene, amphibole and biotite and the LLST contains both nepheline and zircon (Wörner and Schmincke, 1984b). Apatite is present at all levels but is most abundant in the crystal-rich ULST (Wörner and Schmincke, 1984b). The textures and geochemistry of sanidine record strong changes in melt chemistry and are not in equilibrium with the melts in which they erupted, having been brought together from different parts of the system (Ginibre et al., 2004); see also similar interpretations for other phases (Harms et al., 2004; Tait et al., 1989). To date, there has been no detailed study of the apatites and their relationship to the volatile composition of the melt, but there are good constraints on the evolving volatile chemistry of the melt phase, which varies strongly as a function of stratigraphic position (Harms et al., 2004; Harms and Schmincke, 2000; Wörner and Schmincke, 1984b). This makes the Laacher See Tephra an ideal case study for investigating volatile evolution in apatite.

We sampled juvenile material from five levels of the Laacher See Tephra corresponding to sub-units II (LST3, LLST), VII (LST2, lower MLST), XIV (LST1, upper MLST) and XVII (LST4 and LST5, ULST) of Harms and Schmincke (2000). We extracted apatites in the size fractions 180-250 μm and 45-90 μm using heavy liquids and magnetic separation methods. The crystals are typically euhedral with clearly defined rims; some show oscillatory or core-rim zonation in cathodoluminescence that appears to be unsystematically linked to trace element concentration (Fig. 1).

Major-, minor- and volatile-element compositions of apatites were analysed using a JEOL 8600 electron microprobe at the Research Laboratory for Archaeology and the History of Art, University of Oxford. Apatites were analysed using a 15 kV, 10 nA, 5 μm beam with halogens analysed first. Where possible, crystals were mounted with the c-axis perpendicular to the beam direction, in order to mitigate sample damage from the electron beam (Goldoff et al., 2012; Stock et al., 2015; Stormer et al., 1993). Peak counting times were 20-30 s for major elements and 30-90 s for minor elements (120 s for Cl and S). Well-characterised, oriented Wilberforce, Durango and Bamble apatites were used as secondary standards.

Volatile concentrations (H, C, F and Cl) and some trace elements (Mn, Y) were also determined directly in apatite by secondary ion mass spectrometry (SIMS) using a Cameca ims-4f instrument at the NERC Edinburgh Ion Microprobe Facility, University of Edinburgh (see Riker et al., 2018). Volatile contents were determined by constructing working curves with independently characterised

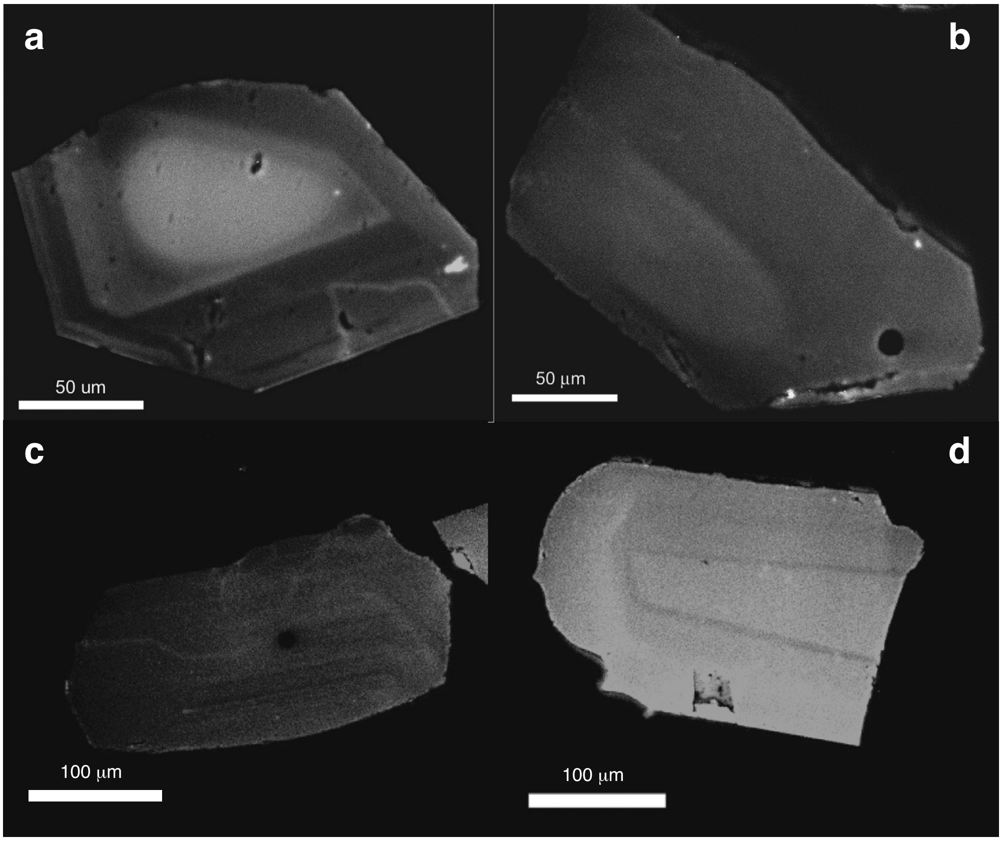

Fig. 1. CL images showing representative Laacher See apatite microphenocrysts with clear euhedral rims and variable degrees of internal zonation.

standards, on the basis of 55 wt% CaO. Halogen contents from EPMA and SIMS agree well (Supplementary information), but with a tendency for EPMA to slightly overestimate the halogen contents due migration under the electron beam (Stock et al., 2015), emphasising the need for SIMS.

4. Results

The apatites in the Laacher See Tephra typically have X_F^{ap} from 0.43–0.67, X_{Cl}^{ap} of 0.042–0.067, X_{OH}^{ap} from 0.31–0.51 (with a stoichiometric volatile site sum of 1.0 calculated as $Ca(PO_4)(OH,F,Cl)$, Supplementary data table). Where the volatile contents of cores and rims were analysed in the same crystal, these are typically the same within error and there is no systematic compositional difference between cores and rims (i.e., cores are not systematically F-enriched or F-depleted relative to rims). In general, the apatite volatile ratios show an ‘inverted V’ shape in plots of X_{Cl}/X_{OH} *vs* X_F/X_{OH} or X_F/X_{Cl} (Fig. 2), with a long tail towards high X_F/X_{Cl} or X_F/X_{OH} and low X_{Cl}/X_{OH} that results from a few of the apatites recording anomalously F-rich, OH-poor and Cl-poor apatite compositions. A small minority of crystals shows elevated X_{Cl}/X_{OH} (Fig. 2). In ternary space, the data dominantly show a trend towards the X_F apex at nearly constant X_{Cl} contents; the break in slope marked by decreasing X_{Cl} is clearly seen (Fig. 3). Carbonate contents are small, with $X_{CO_3^{2-}}^{ap}$ from 0.008-0.024, and sulphur contents are typically in the range 0.55-1.10 wt% SO_2 (Supplementary information). There are no systematic stratigraphic variations in volatile composition, with each individual hand sample recording a wide range of apatite compositions (Fig. 2). In detail, ULST samples overall have a greater proportion of apatites with very low X_F/X_{OH} compositions, resulting in a subtle bimodality (Fig. 2), whereas LLST samples have fewer apatites with very low X_F/X_{OH}, but more with very low X_{Cl}/X_{OH} and higher X_F/X_{OH} and X_F/X_{Cl} ‘evolved’ compositions. However, given the very strong, systematic changes in melt volatile contents throughout the stratigraphy (Harms and Schmincke, 2000; Textor et al., 2003; Tomlinson et al., 2020; Wörner and Schmincke, 1984b) the wide distribution of volatile compositions and lack of equivalent strong, systematic variation in apatite compositions demonstrates a lack of volatile equilibrium between crystals and their carrier liquids.

Apatite trace element concentrations are widely variable, with typically 0.10–0.28 wt% Na_2O, 0.4–0.7 wt% SiO_2 and up to 0.15 wt% MnO, but with no systematic stratigraphic variations and a very wide spread of compositions in any individual hand sample (Fig. 4; Supplementary material). With increasing incompatible element abundance (e.g. Mn, La, Ce), Sr contents increase to a maximum of ∼0.5 wt% SrO before decreasing to very low values (Fig. 4). The ULST samples overall have a greater proportion of apatites with very low incompatible element abundances, whereas LLST samples tend to have more apatites with higher Mn and Ce (Fig. 4). Trace element partitioning behaviour between apatite and the evolving melt could change significantly during fractionation from basanite to phonolite (Prowatke and Klemme, 2006; Stokes et al., 2019), so we have not inverted for the equilibrium melt trace element compositions. As with the volatiles, given the strong stratigraphic variations in matrix glass trace element contents (Tomlinson et al., 2020; Wörner and Schmincke, 1984b), the wide range of apatite trace element compositions seen in each sample indicates that the apatites are out of trace element equilibrium with their carrier liquids. This is similar to interpretations for other magmatic mineral phases and their inclusions (Ginibre et al., 2004; Harms and Schmincke, 2000; Wörner et al., 1983).

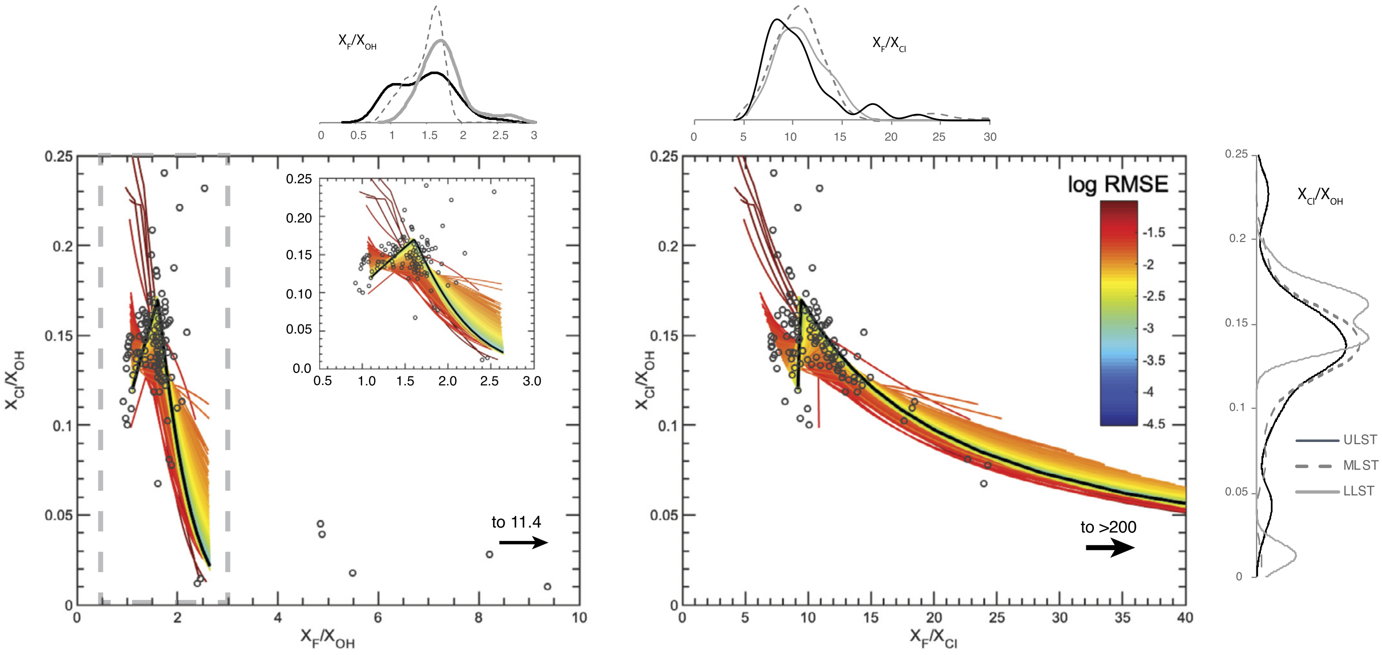

Fig. 2. Laacher See apatite volatile compositions (small grey circles) plotted as mole fraction ratios X_{Cl}/X_{OH} vs X_F/X_{OH} (left) and X_{Cl}/X_{OH} vs X_F/X_{Cl} (right) and the preferred model fit (black line; black outline square shows the starting position for the model). A small number of outlier apatites reach higher X_F/X_{OH} (to 11.4) and X_F/X_{Cl} (to >200), as indicated by the black arrows. Adjacent to the axes are kernel density estimates of the populations for ULST (solid black line), MLST (dashed grey line) and LLST (solid grey line). Also shown are the results of `multistart` modelling as described in the text, coloured by root mean square error (log(RMSE); lower values, blue-yellow, indicate a closer fit to the modelled trend). Runs with very low RMSE (greens and blue) almost completely underlie the black preferred model fit.

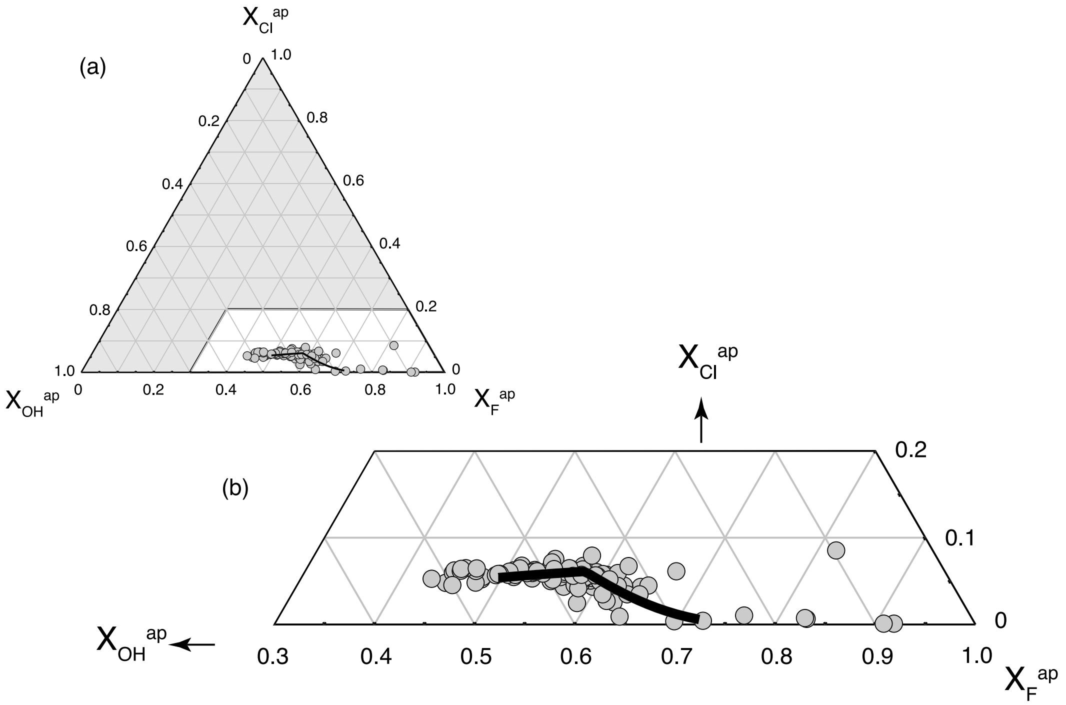

Fig. 3. Ternary figure showing apatite volatile compositions (small grey circles) and the preferred model fit (black line).

5. Volatile modelling results

Our model can quantitatively reproduce the observed apatite volatile trend (solid black line, Fig. 2; Fig. 3). Starting from low X_F/X_{OH}, the initial increase in halogen/OH ratios occurs during volatile-undersaturated fractionation. The sharp break in slope (at $X_{Cl}/X_{OH} \sim 0.17$) coincides with the onset of volatile-saturated conditions in the model and is followed by decreasing X_{Cl}/X_{OH}, which is generated as chlorine begins to be extracted into an exsolving fluid. Our preferred best fit model result (Fig. 2; Fig. 3) requires a low initial melt H_2O concentration (1.5 wt%), low crystal-melt partition coefficients for H_2O ($D_{H_2O}^{xl-m} = 0.12$), Cl ($D_{Cl}^{xl-m} = 0.05$) and F ($D_F^{xl-m} = 0.10$), and a high fluid-melt partition coefficient for Cl (Table 1). The crystal-melt partition coefficients are reasonable considering a fractionating assemblage of ~80% sanidine, ~5-6% amphibole, ~1% haüyne and ~0.5% apatite (Wörner and Schmincke, 1984b) and using realistic estimates for the volatile

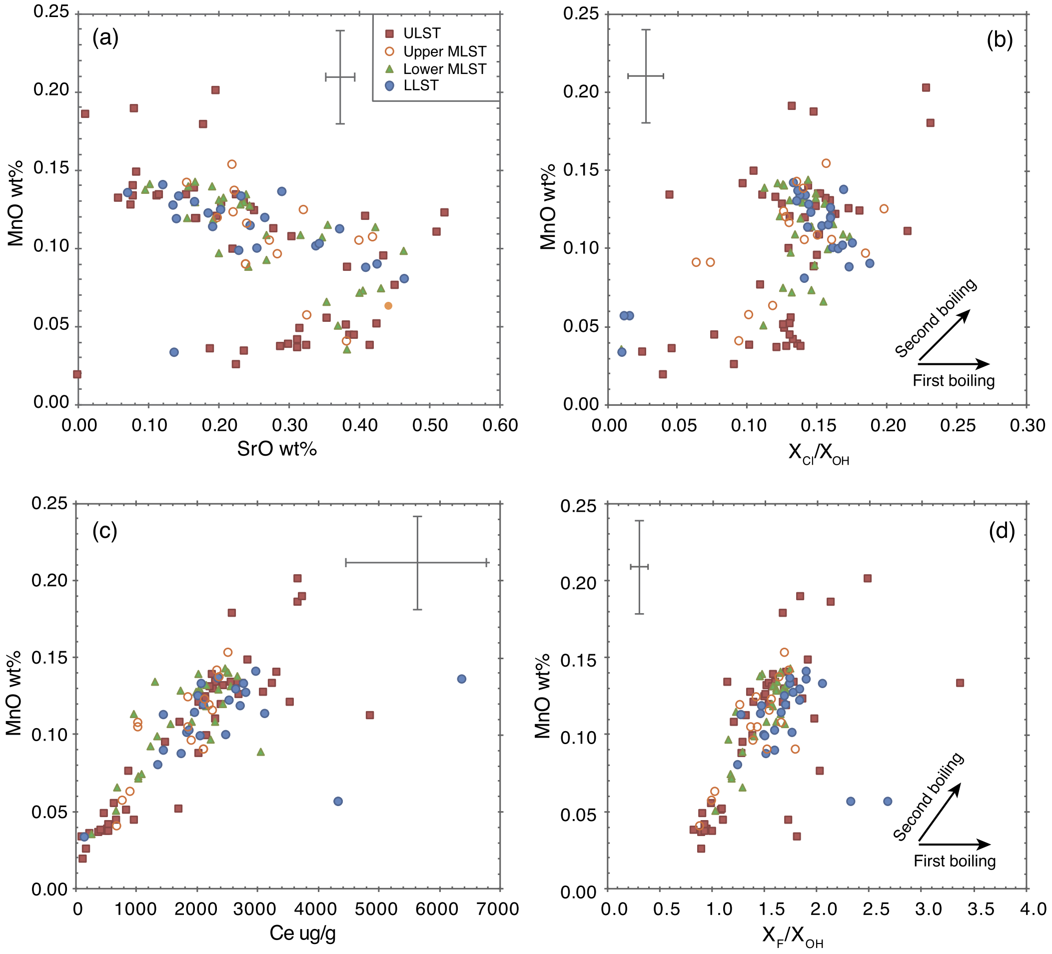

Fig. 4. Laacher See apatite trace element and volatile compositions as a function of stratigraphic height. 1σ analytical uncertainties are indicated on each panel. Qualitative trends expected for first and second boiling are shown in panels (b) and (d). (For interpretation of the colours in the figure(s), the reader is referred to the web version of this article.)

Table 1
Parameter values used for our preferred 'best fit' model run.

Initial melt volatile concentrations	
Cl wt%	0.14
F wt%	0.11
H_2O wt%	1.5
H_2O saturation level	
H_2O wt%	5.6
Bulk crystal-melt partition coefficients	
Cl	0.05
F	0.1
H_2O	0.12
Bulk fluid-melt distribution coefficients	
Cl	40
F	2
Apatite-melt exchange coefficients	
Cl-F	0.1
Cl-OH	10
F-OH	23

compositions of the amphibole and haüyne. Our modelled initial melt has 1400 ppm Cl and 1100 ppm F, with vapour saturation pre-defined at 5.6 wt% H_2O (Table 1; equivalent to magma storage at ~130 MPa using Schmidt and Behrens, 2008). The combination of low initial melt H_2O concentration and high storage pressure means that the initial melt was volatile-undersaturated, consistent with high-temperature phase equilibrium experiments (Harms et al., 2004).

We also used the thermodynamic non-ideal mixing model of Li and Costa (2020) to estimate the initial melt volatile composition, for comparison with our ideal mixing approach. We chose an apatite composition close to the start of our modelled trend, with $X_{Cl}/X_{OH} = 0.128$ and $X_F/X_{OH} = 1.277$. Assuming a temperature of 1100 °C and melt halogen contents of 1400 ppm Cl and 1100 ppm F (see above), the Li and Costa (2020) model returns a melt H_2O concentration of 1.6 wt% H_2O, which compares well with our modelled value (1.5 wt%). This suggests that the degree of non-ideality in the system may be minor (Hovis et al., 2015, 2014). However, choosing a lower temperature yields a result that is significantly different and we suggest that further work, including additional apatite-melt partitioning experiments, is needed to clarify these effects.

5.1. Sensitivity analysis

Our preferred best fit model trend gives a good match to the measurements of apatite composition. However, because competition for space in the apatite channel volatile site is controlled by exchange reactions (i.e., if the volatile site is filled by fluorine, for example, then there is less room for OH and chlorine to enter the site), our model results are inherently non-unique. In other words, the values of the starting parameters used are not the only possible set of values that could generate a good fit to the data. We have therefore developed a sensitivity analysis approach to determine how much potential co-variation there may be between different starting parameter values.

The Laacher See apatite volatile compositions do not vary monotonically (i.e., they increase to a peak in X_{Cl}/X_{OH} and then decrease again) and RMSE is computed by interpolation, so it is difficult to search for multiple solutions by minimising to the underlying dataset. We therefore used the MATLAB `multistart` global optimisation function to investigate multiple local minima around our preferred best fit model trend (or 'target curve'), as outlined earlier. We provided wide bounds to delimit the upper and lower range of the parameter values to be investigated (e.g. 0.1–6.0 wt% H_2O or a factor of ×6 to ×150 variability for all parameters, Appendix Table 1, refer to mmc2). Full details of the `multistart` implementation and results are given in the Appendix, refer to mmc 7 and mmc 8. This sensitivity analysis approach shows how RMSE (i.e., goodness of fit) varies when changing the initial starting parameter values used for successful runs, relative to the preferred best fit model trend. For our Laacher See apatites, the `multistart` output shows that the model runs that fit most closely to our target curve have a narrow distribution of initial melt H_2O concentrations; higher initial melt H_2O concentrations are associated with increasingly high RMSE (Appendix Fig. 1, refer to mmc 1). This suggests that in this specific example, the model result is relatively sensitive to this parameter (in other words, our estimated initial melt H_2O content is relatively well defined), because evolving from H_2O-undersaturated to H_2O-saturated conditions generates a distinct break in slope in both dataset and model. Conversely, the best fitting model runs show a much broader spread of initial melt halogen concentrations because of the non-uniqueness in the system of equations. The full `multistart` output data (Supplementary material) can be used to identify that, for the best fitting model runs in this example, changing the initial melt Cl concentration is accommodated by varying K^{ap-m}_{Cl-OH}; variations in the initial melt F content can be accommodated by varying K^{ap-m}_{F-OH} and K^{ap-m}_{Cl-F} (and to a lesser extent, D^{xl-m}_{F} and $D^{xl-m}_{H_2O}$). In this example, successful solutions can also have different initial melt H_2O concentrations, but this covaries strongly with all the crystal-melt partition coefficients because the position of the break in slope depends on both the pre-defined H_2O saturation limit (which is not a variable in the `multistart` function) and D^{xl-m}_{i}. A higher initial melt H_2O concentration is still plausible, but this would require deeper magma storage (higher $C^{sat}_{H_2O}$) in order to prevent much earlier volatile saturation in the magma. Interestingly, the modelled fluid-melt partition coefficient for Cl (D^{fl-m}_{Cl}) is typically in the range 30-50 for successful runs, consistent with experimental work (e.g. Kravchuk and Keppler, 1994; Webster, 1992) but D^{fl-m}_{F} is also universally >1 in the successful runs (Appendix Fig. 1, refer to mmc1), indicating some loss of fluorine into the evolving fluid. This contrasts with Harms and Schmincke (2000), who suggested that F is retained in the melt, but is consistent with experimental constraints on volatile behaviours in phonolite liquid (Chevychelov et al., 2008). To summarise: running the `multistart` sensitivity analysis function allows the user to understand the limitations on plausible bounds of initial parameter values. Petrological constraints appropriate to the specific system of interest can be applied to the `multistart` results to gain further insights into the nature of the magmatic system.

5.2. Comparison with petrologic data

One of the advantages of the Laacher See system is the well understood variations in glass chemistry, including volatile concentrations in melt inclusions and matrix glasses (Harms and Schmincke, 2000; Textor et al., 2003; Tomlinson et al., 2020). This allows us to validate our preferred model result(s) for the melt phase against direct measurements of the glass. Following Harms and Schmincke (2000), we use Na_2O/K_2O as a general measure of melt evolution, and link this to our modelled F based on a regression against Zr concentrations from Tomlinson et al. (2020), assuming an initial melt Zr content (C_0) of 300 ppm and perfectly incompatible behaviour ($D = 0$). Our modelled melt volatile compositions compare well with published matrix glass and melt inclusion measurements (Fig. 5). This shows that our preferred best fit model trend, defined by reproducing the volatile chemistry of apatites, gives a very good match for petrological observations. The least evolved melt inclusions have 1.3–2.0 wt% H_2O, 1700–2700 ppm Cl and 700–1900 ppm F (Harms and Schmincke, 2000), in good agreement with the initial melt composition from our preferred best-fit model. Fluorine contents of matrix glasses increase continuously to reach >7000 ppm in the most evolved melts (Harms and Schmincke, 2000); our model similarly reaches 7779 ppm fluorine at F (fraction of melt remaining) = 0.1 (Fig. 5). In contrast, Cl concentrations reach a maximum of ~6000 ppm in lower MLST matrix glasses and then decline towards ~1000 ppm in the most evolved melts (Harms and Schmincke, 2000; Tomlinson et al., 2020; Wörner and Schmincke, 1984b). Our modelled melt Cl reaches 5720 ppm at $F = 0.22$ when vapour saturation occurs, and then declines to 934 ppm at $F = 0.1$ (Fig. 5). This late-stage pre-eruptive volatile evolution is not recorded by the melt inclusions (Harms and Schmincke, 2000) but is recorded in the apatite. Overall, we infer that melts equivalent to lower MLST and LLST were volatile-saturated whereas upper MLST and ULST melts were volatile-undersaturated (Fig. 5).

6. Discussion

6.1. Evolution of magmatic vapour during fractionation

Our new apatite data and modelling shows that the evolving volatile composition of the Laacher See melt can largely be reproduced through fractional crystallisation. This does not exclude any influx of new melts into the system during magma evolution (e.g. Wörner and Wright, 1984; Tomlinson et al., 2020) but suggests that any recharge or mixing events probably involved melts on a similar liquid line of descent to the main phonolite sequence. The melt was initially strongly volatile-undersaturated and became vapour-saturated during fractionation. Exsolution of H_2O-rich vapour stripped Cl from the melt, reducing the Cl concentrations of the evolving melt and generating the observed Cl-depleted matrix glass. Fluorine was only minimally extracted from the melt into the vapour: because of the low bulk partition coefficient for all phases (crystals and fluid), fluorine concentrations continued to increase in the evolving liquid after vapour saturation. Using X_F/X_{OH} as an indication of the stage of volatile evolution, it is clear that enrichment of incompatible trace elements (e.g. Mn, Ce) accompanied volatile fractionation, albeit with some scatter (e.g. Fig. 4d). This suggests that vapour saturation was mostly achieved through second boiling, with progressive volatile and trace element enrichment taking place *in situ* during storage and fractionation. A scenario with local, lateral variations in crystallinity, in multiple small melt lenses at similar storage pressures, would also be consistent with the data. We cannot exclude limited pressure variations within the precision of the dataset, but a strong control by first boiling would be expected to generate significant variations in Cl/OH with little change in trace elements (Fig. 4). A few apatite crystals have anomalously high $X_F/X_{OH} > 6$ and $X_F/X_{Cl} > 50$, and a few have higher X_{Cl}/X_{OH} (see Supplementary data table; Fig. 2). These scattered outlier compositions are likely the result of more extensive fractionation, or re-equilibration during cooling. Following Stock et al. (2018), we therefore suggest that these crystals

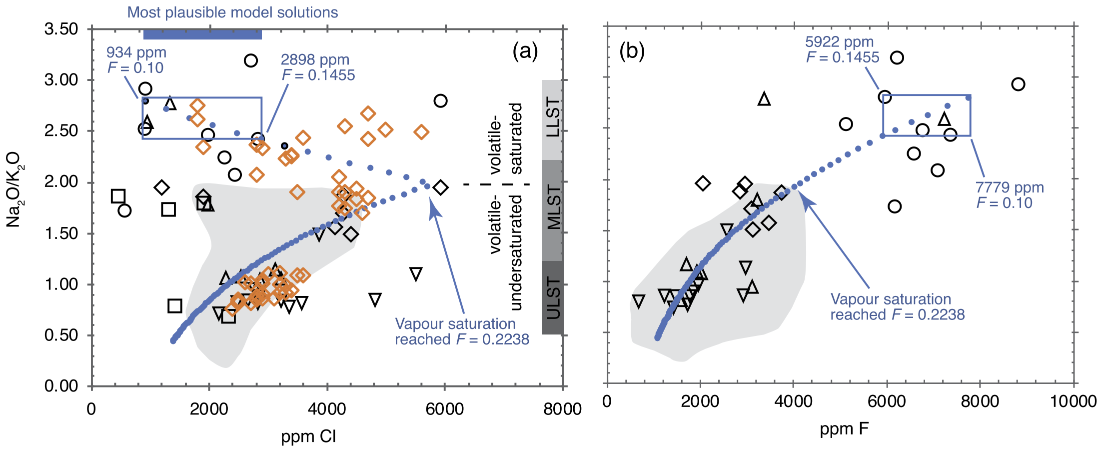

Fig. 5. Variation of melt volatile composition during progressive fractional crystallisation (blue dots) as a function of melt evolution for our preferred model trend (with melt evolution expressed as Na_2O/K_2O following Harms and Schmincke, 2000). Also shown are data for melt inclusions (grey field) and matrix glasses (black open symbols) after Harms and Schmincke (2000, Figs 6 and 7; circles – LLST; squares, diamonds and upward triangles – MLST; downward triangles – ULST). Open diamonds in orange are matrix glasses from Tomlinson et al. (2020). The blue filled box indicates the range of plausible model end points between $F = 0.1455$ (Cl = 2898 ppm and $F = 5922$ ppm) and $F = 0.100$ (Cl = 934 ppm and $F = 7779$ ppm) based on comparison to measured matrix glass compositions from the literature. The modelled reversal in (a) indicates the point of volatile saturation as indicated on the schematic stratigraphic column, which is reached when $F = 0.2238$ in our preferred model.

may have been scavenged from fragments of older crystalline material incorporated during eruption. Overall, our new finding, that the magma was initially volatile-undersaturated and reached saturation through fractionation, is significant and raises the possibility that growth and expansion of an exsolved volatile phase within the crystal mush could be implicated in triggering eruptions.

6.2. Rapid destabilisation of a crystal mush column

The Laacher See apatite crystals preserve a wide range of compositions in each hand sample, and are not in equilibrium with their carrier volcanic melts. This requires the apatite crystals to be dispersed or redistributed within the compositionally variable melt, as shown for other phases (Ginibre et al., 2004; Tait et al., 1989). The (weakly) bimodal trace element and volatile compositions of apatites from the ULST are consistent with episodes of recharge with primitive (basanite) melts into the ULST magma, as indicated by compositional heterogeneity in the glasses (Tomlinson et al., 2020), variable composition of ferromagnesian minerals (Berndt et al., 2001), and the presence of mingled clasts (Wörner and Wright, 1984). Apatites from LLST samples tend to record more restricted compositions with slightly higher incompatible element concentrations (see Fig. 3), indicating growth from a more evolved melt. This suggests that the LLST melt was separated from more primitive parts of the magmatic system and evolved as a separate melt lens, perhaps within a spatially discrete part of a mushy plumbing system. Although there are differences in crystal abundance and the distribution of apatite compositions from ULST and LLST, it is notable that all samples contain crystals covering the full compositional range observed. This indicates that eruption involved (or was preceded by) a significant rearrangement of the evolving magmatic system. We interpret this as wide-ranging structural reorganisation of an extensive, crystal-rich mush that contained multiple disseminated melt lenses (e.g. Christopher et al., 2015). This is consistent with evidence from the distribution and compositional heterogeneity of matrix glasses (Tomlinson et al., 2020) and other studies on compositional and textural heterogeneity of different mineral phases (e.g. sanidine, Ginibre et al., 2004; clinopyroxene, Wörner and Wright, 1984). Given the clear evidence that vapour saturation occurred during fractional crystallisation, we suggest that growth of vapour bubbles within the crystallising mush framework could have helped to destabilise and remobilise the magma (Truby, 2016).

Table 2
First-order estimates of diffusive equilibration timescales for small apatite crystals 45-90 μm in diameter, or rims of larger crystals, using diffusivity data from Brenan (1993).

	900 (°C)	800 (°C)	700 (°C)
D $\mu m^2/s$ (1 GPa)	1.601E-15	3.065E-16	4.176E-17
t (22.5 μm), days	0.9	5	35
t (45 μm), days	3.7	19	140
t (≤20 μm from rim), days	0.7	4	28

Importantly, the observation that the apatites are also out of equilibrium with the volatile contents of their carrier liquids (because each sample contains well-defined melt volatile contents but a wide range of apatite compositions, Fig. 2) can provide additional insights into the structural origins of the crystals within the plumbing system. By recognising the high diffusivities of volatile species in apatite (Boyce and Hervig, 2009, 2008; Brenan, 1993; Higashi et al., 2017; Li et al., 2020), we can place new first-order constraints on the timescales of the structural mush reorganisation process. The smaller population of crystals (45-90 μm) show no systematic difference in volatile composition from the larger crystals (180-250 μm), and cores and rims of the same larger crystals (rims measured ≤20 μm from the edge of the grain) were also not systematically different. For a spherical particle of radius r:

$$r \approx (4Dt)^{\frac{1}{2}}$$

where D is the diffusivity and t is the time taken for 95% of net chemical exchange towards complete equilibration (Crank, 1975; Hofmann, 1980). As we see no systematic core-rim variations in our apatites, the relevant lengthscale is the radius of the smaller crystals (i.e. 22.5-45 μm) or the distance of the analysis from the rims of the larger grains (≤20 μm). We use the 1 GPa hydrothermal diffusivities measured experimentally by Brenan (1993), which are suitable for H_2O-bearing melts, to derive a first-order estimate of the equilibration time. For conservative temperatures of ~700 °C, suitable for the most evolved phonolite (Tomlinson et al., 2020), characteristic equilibration times are on the order of 1-5 months (35-140 days, Table 2). At slightly higher temperatures, which would be appropriate for less evolved parts of the mushy storage system (because trace element contents indicate that many of the apatites are derived from hotter, more primitive melts) timescales could be as short as 1-4 days (Table 2). These timescales are similar to those defined by diffusion modelling of both olivine and sanidine (10-400 days; Rout and Wörner, 2018; Sundermeyer et al., 2020). This means that the dispersal of crystals and reorganisation of the plumbing system structure took place on short timescales prior to eruption, from perhaps only a few days to a maximum of a few months. This finding is important because it suggests that any pre-eruptive surface monitoring signals of either new basanite melt intrusion or structural rearrangements of the crustal plumbing system, if a similar eruption were to happen today, would be expected to occur immediately before eruption. These are relatively conservative estimates because many of the apatites will be derived from hotter, more primitive melts. More experimental work on apatite volatile diffusivities in hydrous melts at crustal pressures is needed to constrain these timescales further.

6.3. Volatile emissions and atmospheric loading from the Laacher See eruption

The results of our apatite volatile modelling allow us, for the first time, to estimate the contribution that pre-eruptive exsolved gases make to overall volatile emissions from the eruption. Volatile emissions are commonly characterised using the 'petrologic method'. This method works by estimating the extent of syn-eruptive degassing based on the difference between pre-eruptive dissolved volatile contents, measured in melt inclusions, and degassed matrix glass volatile concentrations (e.g. Harms and Schmincke, 2000). Such methods typically underestimate the overall emissions because they cannot account for any pre-existing exsolved vapour; this effect is one cause of the common observation of "excess sulphur" emissions compared with satellite-derived observations. The volatile composition of apatite appears to be quite sensitive to the onset of fluid exsolution (see Fig. 2), and we now use the apatite and melt modelling results to calculate directly the mass and composition of pre-eruptive exsolved fluid.

Following Harms and Schmincke (2000), we take the total erupted melt mass of the LLST and lower MLST (which reached volatile saturation, as inferred from Fig. 5) as 9.01×10^{12} kg. Reasonable model outputs are reached between the modelled volatile contents and Cl and F contents of matrix glasses for $0.1455 < F < 0.1$ (Fig. 5) so we use these limits on F to calculate a lower and upper bound for the composition and volume of vapour exsolved. We use the following step-wise approach as a function of Z (the fraction of volatile-saturated melt remaining), after Candela and Holland (1986):

Mass (kg) of exsolved H_2O as a function of Z:

$$\mathrm{H_2O}^{fl}(Z) = \sum_{Z} \left[\left(C^{m}_{\mathrm{H_2O}} - C^{\mathrm{sat}}_{\mathrm{H_2O}} \right) \times \mathrm{mass}(m) \times Z^{i} \right]$$

where $C^{m}_{H_2O}$ is the wt fraction of H_2O in the melt if there were no exsolved fluid, $C^{\mathrm{sat}}_{H_2O}$ is the wt fraction of H_2O in the melt at volatile saturation, and m is melt.

Then the mass (kg) of exsolved Cl in the fluid is calculated as:

$$\begin{aligned} \mathrm{Cl}^{fl}(Z) &= \sum_{Z} \left[\left(C^{fl}_{\mathrm{Cl}} - \mathrm{H_2O}^{fl}(Z) \right) \times Z^{i} \right] \\ &= \sum_{Z} \left[\left(\left(C^{m}_{\mathrm{Cl}} \cdot D^{fl}_{\mathrm{Cl}} \right) - \mathrm{H_2O}^{fl}(Z) \right) \times Z^{i} \right] \end{aligned}$$

The mass of exsolved fluorine in the melt is calculated in a similar way. In total we calculate that for the upper bound $F = 0.1455$, the pre-eruptive vapour released during the eruption would contain 187 Tg H_2O, 26.2 Tg Cl and 1.5 Tg F. For the lower bound $F = 0.10$, the pre-eruptive vapour released would contain 339 Tg H_2O, 31.8 Tg Cl and 2.7 Tg F. For Cl, this approach implicitly assumes that the decline in melt Cl concentrations from peak levels in lower MLST to the levels seen in LLST matrix glasses (Fig. 5) is due to pre-eruptive volatile exsolution. This is in contrast to the 'petrologic method' approach of Harms and Schmincke (2000), which assumes that this decrease happens syn-eruptively. Significant syn-eruptive degassing of chlorine is problematic given the rather slow diffusivity in phonolite melts (2 orders of magnitude lower diffusivity than H_2O, and at least a factor x5 lower than diffusivity of fluorine in phonolite melt at the same temperature, Böhm and Schmidt, 2013), so we suggest that pre-eruptive volatile exsolution is a more reasonable interpretation. Conversely, our calculated pre-eruptive exsolved H_2O mass is *in addition* to the 403 Tg calculated (using the petrologic method) to have degassed syn-eruptively (Harms and Schmincke, 2000). Furthermore, the syn-eruptive H_2O degassing calculated from LLST and lower MLST by Harms and Schmincke (2000) assumed a pre-eruptive H_2O concentration of 3.61 wt% H_2O, whereas our calculations suggest a much higher value of 5.6 wt% (i.e., our pre-defined H_2O saturation level that generates a good modelled match to the data). Updating their petrologic method calculations based on this new value gives a total of 582 Tg H_2O released by syn-eruptive degassing, or 769-921 Tg H_2O released during the course of the eruption (including both syn-eruptive degassing and loss of pre-eruptive stored vapour). We note that performing a similar analysis using sulphur contents of apatite is not meaningful because of the presence of sulphur-bearing phases (early pyrrhotite and later haüyne and cancrinite; Harms and Schmincke, 2000; Wörner and Schmincke, 1984b) as well as the documented change in oxidation state during fractionation (Harms and Schmincke, 2000) which strongly affects the partitioning of sulphur (Peng et al., 1997).

These calculations, using our apatite modelling, increase the inferred atmospheric loading by $>$90% for H_2O and by $\geq$300% for Cl compared with previous estimates (Harms and Schmincke, 2000). The calculations also show that F emissions can be considerable (up to 2.7 Tg) if a pre-eruptive vapour is present, even if fluorine concentrations are not decreasing in the evolved matrix melt prior to or during eruption. Using an alternative petrologic method approach based on comparison to bromine, Textor et al. (2003) also estimated a relatively large mass release during the same eruption of 11.5 Tg Cl, 0.2 Tg F and 698 Tg H_2O. Although halogens may be partially scrubbed from volcanic plumes by condensation onto tephra particles, incorporation into ice or reaction (e.g. Textor et al., 2003), our new apatite volatile data and modelling indicates a substantial input of reactive halogen-bearing gas into the stratosphere, where significant ozone depletion could occur (Brasseur and Granier, 1992). This demonstrates the importance of recognising and quantifying the potentially very significant contribution of pre-eruptive exsolved gas in the emissions of explosive volcanic eruptions.

7. Conclusions

Apatite volatile compositions are sensitive to the onset of volatile saturation in magmas, providing new constraints on the pressure of magma storage and the possible role of volatile exsolution in pre-eruptive processes. Apatites from the Laacher See magma record initially volatile-undersaturated fractional crystallisation, followed by second boiling. Forward modelling can quantitatively reproduce the measured apatite compositions, and produce model results that agree well with existing matrix glass measurements from Laacher See tephra. A new sensitivity analysis allows an understanding of the effects of non-uniqueness in the apatite-melt-fluid system. The apatites are not in volatile or trace element equilibrium with their carrier liquids, indicating transfer into new chemical environments shortly before eruption. This dispersal of the crystals throughout the zoned Laacher See volcanic system likely occurs by destabilisation and reorganisation of the mushy plumbing system only a few months prior to the explosive eruption. Finally, the forward model allows a direct measure of the contribution of pre-exsolved gas to atmospheric loading during the eruption, which shows significant emissions of HF and H_2O that have not previously been accounted for. Analysis of volatiles in apatite thus has great potential for bringing new insights into physical volcanology as well as the pre-eruptive volatile compositions of magmas and coexisting fluids.

Declaration of competing interest

The authors declare that they have no known competing financial interests or personal relationships that could have appeared to influence the work reported in this paper.

Acknowledgements

We thank Roel van Elsas for support during work at the Mineral Separation Laboratory, Vrije Universiteit Amsterdam, and Fabian Wadsworth for helpful discussions. We acknowledge useful comments from two anonymous reviewers which helped to improve this work.

Funding: This work was supported by the Natural Environment Research Council [grant numbers NE/N002954/1, NE/K003852/1 and /2, NE/KS00811/01, and NE/R011389/1]. Humphreys was supported by a Royal Society University Research Fellowship [grant number UF140711]. This project has also received funding from the European Research Council (ERC) under the European Union's Horizon 2020 research and innovation programme [grant agreement No. 864923]. We also acknowledge support from the NERC ion microprobe facility [grant number IMF549/1114].

Appendix A. Supplementary material

Supplementary material related to this article can be found online at https://doi.org/10.1016/j.epsl.2021.117198.

References

Berndt, J., Holtz, F., Koepke, J., 2001. Experimental constraints on storage conditions in the chemically zoned phonolitic magma chamber of the Laacher See volcano. Contrib. Mineral. Petrol. 140, 469–486. https://doi.org/10.1007/PL00007674.

Böhm, A., Schmidt, B.C., 2013. Fluorine and chlorine diffusion in phonolitic melt. In: 9th Silicate Melts Workshop. Chem. Geol. 346, 162–171. https://doi.org/10.1016/j.chemgeo.2012.09.005.

Boudreau, A.E., McCallum, I.S., 1989. Investigations of the stillwater complex, part V: Apatites as indicators of evolving fluid composition. Contrib. Mineral. Petrol. 102, 138–153.

Boyce, J.W., Hervig, R.L., 2009. Apatite as a monitor of late-stage magmatic processes at Volcán Irazú, Costa Rica. Contrib. Mineral. Petrol. 157, 135–145. https://doi.org/10.1007/s00410-008-0325-x.

Boyce, J.W., Hervig, R.L., 2008. Magmatic degassing histories from apatite volatile stratigraphy. Geology 36, 63. https://doi.org/10.1130/G24184A.1.

Boyce, J.W., Tomlinson, S.M., McCubbin, F.M., Greenwood, J.P., Treiman, A.H., 2014. The Lunar Apatite Paradox. Science 344, 400–402. https://doi.org/10.1126/science.1250398.

Brasseur, G., Granier, C., 1992. Mount Pinatubo aerosols, chlorofluorocarbons, and ozone depletion. Science 257, 1239–1242.

Brenan, J., 1993. Kinetics of fluorine, chlorine and hydroxyl exchange in fluorapatite. Chem. Geol. 110, 195–210.

Candela, P.A., 1986. Towards a thermodynamic model for the halogens in magmatic systems: an application to melt-vapor-apatite equilibria. Chem. Geol. 57, 289–301.

Candela, P.A., Holland, H.D., 1986. A mass transfer model for copper and molybdenum in magmatic hydrothermal systems: the origin of porphyry-type ore deposits. Econ. Geol. 81, 1–19.

Cashman, K.V., Sparks, R.S.J., Blundy, J.D., 2017. Vertically extensive and unstable magmatic systems: a unified view of igneous processes. Science 355, eaag3055.

Christopher, T.E., Blundy, J., Cashman, K., Cole, P., Edmonds, M., Smith, P.J., Sparks, R.S.J., Stinton, A., 2015. Crustal-scale degassing due to magma system destabilization and magma-gas decoupling at Soufriere Hills Volcano, Montserrat. Geochem. Geophys. Geosyst. 16, 2797–2811. https://doi.org/10.1002/2015GC005791.

Crank, J., 1975. The Mathematics of Diffusion. Oxford Science Publications. Clarendon Press, Oxford [England]. 1916-.

Doherty, A.L., Webster, J.D., Goldoff, B.A., Piccoli, Philip M., 2014. Partitioning behavior of chlorine and fluorine in felsic melt-fluid(s)-apatite systems at 50 MPa and 850-950 °C. Chem. Geol. 384, 94–111.

Douce, A.E.P., Roden, M.F., Chaumba, J., Fleisher, C., Yogodzinski, G., 2011. Compositional variability of terrestrial mantle apatites, thermodynamic modeling of apatite volatile contents, and the halogen and water budgets of planetary mantles. Chem. Geol. https://doi.org/10.1016/j.chemgeo.2011.05.018.

Ginibre, C., Wörner, G., Kronz, A., 2004. Structure and Dynamics of the Laacher See Magma Chamber (Eifel, Germany) from Major and Trace Element Zoning in Sanidine: a Cathodoluminescence and Electron Microprobe Study. J. Petrol. 45, 2197–2223. https://doi.org/10.1093/petrology/egh053.

Goldoff, B., Webster, J.D., Harlov, D.E., 2012. Characterization of fluor-chlorapatites by electron probe microanalysis with a focus on time-dependent intensity variation of halogens. Am. Mineral. 97, 1103–1115. https://doi.org/10.2138/am.2012.3812.

Harms, E., Gardner, J.E., Schmincke, H.-U., 2004. Phase equilibria of the Lower Laacher See Tephra (East Eifel, Germany): constraints on pre-eruptive storage conditions of a phonolitic magma reservoir. J. Volcanol. Geotherm. Res. 134, 125–138.

Harms, E., Schmincke, H.-U., 2000. Volatile composition of the phonolitic Laacher See magma (12,900 yr BP): implications for syn-eruptive degassing of S, F, Cl and H_2O. Contrib. Mineral. Petrol. 138, 84–98.

Higashi, Y., Itoh, S., Hashiguchi, M., Sakata, S., Hirata, T., Watanabe, K., Sakaguchi, I., 2017. Hydrogen diffusion in the apatite-water system: fluorapatite parallel to the c-axis. Geochem. J. 51, 115–122.

Hofmann, A.W., 1980. Chapter 9: Diffusion in natural silicate melts: a critical review. In: Physics of Magmatic Processes. Princeton University Press, pp. 385–418.

Hovis, G., Abraham, T., Hudacek, W., Wildermuth, S., Scott, B., Altomare, C., Medford, A., Conlon, M., Morris, M., Leaman, A., Almer, C., Tomaino, G., Harlov, D., 2015. Thermal expansion of F-Cl apatite crystalline solutions. Am. Mineral. 100, 1040–1046.

Hovis, G.L., McCubbin, F.M., Nekvasil, H., Ustunisik, G., Woerner, W.R., Lindsley, D.H., 2014. A novel technique for fluorapatite synthesis and the thermodynamic mixing behavior of F-OH apatite crystalline solutions. Am. Mineral. 99, 890–897. https://doi.org/10.2138/am.2014.4750.

Kravchuk, I.F., Keppler, H., 1994. Distribution of chloride between aqueous fluids and felsic melts at 2 kbar and 800 degrees C. Eur. J. Mineral. 6, 913–923.

Li, W., Chakraborty, S., Nagashima, K., Costa, F., 2020. Multicomponent diffusion of F, Cl and OH in apatite with application to magma ascent rates. Earth Planet. Sci. Lett. 550, 116545. https://doi.org/10.1016/j.epsl.2020.116545.

Li, W., Costa, F., 2020. A thermodynamic model for F-Cl-OH partitioning between silicate melts and apatite including non-ideal mixing with application to constraining melt volatile budgets. Geochim. Cosmochim. Acta 269, 203–222.

Li, H., Hermann, J., 2015. Apatite as an indicator of fluid salinity: an experimental study of chlorine and fluorine partitioning in subducted sediments. Geochim. Cosmochim. Acta 166, 267–297.

McCubbin, F.M., Boyce, J.W., Srinivasan, P., Santos, A.R., Elardo, S.M., Filiberto, J., Steele, A., Shearer, C.K., 2016. Heterogeneous distribution of H_2O in the Martian interior: implications for the abundance of H_2O in depleted and enriched mantle sources. Meteorit. Planet. Sci. 51, 2036–2060. https://doi.org/10.1111/maps.12639.

Moore, L.R., Gazel, E., Tuohy, R., Lloyd, A.S., Esposito, R., Steele-MacInnis, M., Hauri, E.H., Wallace, P.J., Plank, T., Bodnar, R.J., 2015. Bubbles matter: an assessment of the contribution of vapor bubbles to melt inclusion volatile budgets. Am. Mineral. 100, 806–823.

Peng, G., Luhr, J.F., McGee, J.J., 1997. Factors controlling sulfur concentrations in volcanic apatite. Am. Mineral. 82, 1210–1224.

Popa, R.-G., Tollan, P., Bachmann, O., Schenker, V., Ellis, B., Allaz, J.M., 2021. Water exsolution in the magma chamber favors effusive eruptions: application of Cl-F partitioning behavior at the Nisyros-Yali volcanic area. Chem. Geol. 570, 120170. https://doi.org/10.1016/j.chemgeo.2021.120170.

Portnyagin, M., Almeev, R., Matveev, S., Holtz, F., 2008. Experimental evidence for rapid water exchange between melt inclusions in olivine and host magma. Earth Planet. Sci. Lett. 272, 541–552. https://doi.org/10.1016/j.epsl.2008.05.020.

Prowatke, S., Klemme, S., 2006. Trace element partitioning between apatite and silicate melts. Geochim. Cosmochim. Acta 70, 4513–4527. https://doi.org/10.1016/j.gca.2006.06.162.

Riker, J., Humphreys, M.C.S., Brooker, R.A., De Hoog, J.C.M., EIMF, 2018. First measurements of OH-C exchange and temperature-dependent partitioning of OH and halogens in the system apatite–silicate melt. Am. Mineral.

Rout, S.S., Wörner, G., 2018. Zoning and exsolution in alkali feldspars from Laacher See volcano (Western Germany): constraints on temperature history prior to eruption. Contrib. Mineral. Petrol. 173, 95. https://doi.org/10.1007/s00410-018-1522-x.

Schmidt, B.C., Behrens, H., 2008. Water solubility in phonolite melts: influence of melt composition and temperature. Chem. Geol. 256, 259–268.

Sparks, R.S.J., 1978. The dynamics of bubble formation and growth in magmas: a review and analysis. J. Volcanol. Geotherm. Res. 3, 1–37.

Stock, M.J., Humphreys, M.C., Smith, V.C., Isaia, R., Brooker, R.A., Pyle, D.M., 2018. Tracking volatile behaviour in sub-volcanic plumbing systems using apatite and glass: insights into pre-eruptive processes at Campi Flegrei, Italy. J. Petrol. 59, 2463–2492.

Stock, M.J., Humphreys, M.C.S., Smith, V.C., Isaia, R., Pyle, D.M., 2016. Late-stage volatile saturation as a potential trigger for explosive volcanic eruptions. Nat. Geosci. 9, 249–255.

Stock, M.J., Humphreys, M.C.S., Smith, V.C., Johnson, R.D., Pyle, D.M., EIMF, 2015. New constraints on electron-beam induced halogen migration in apatite. Am. Mineral. 100, 281–293.

Stokes, T.N., Bromiley, G.D., Potts, N.J., Saunders, K.E., Miles, A.J., EIMF, 2019. The effect of melt composition and oxygen fugacity on manganese partitioning between apatite and silicate melt. Chem. Geol. 506, 162–174. https://doi.org/10.1016/j.chemgeo.2018.12.015.

Stormer, J.C., Pierson, M.L., Tacker, R.C., 1993. Variation of F and Cl X-ray intensity due to anisotropic diffusion in apatite during electron microprobe analysis. Am. Mineral. 78, 641–648.

Sundermeyer, C., Gätjen, J., Weimann, L., Wörner, G., 2020. Timescales from magma mixing to eruption in alkaline volcanism in the Eifel volcanic fields, western Germany. Contrib. Mineral. Petrol. 175, 77. https://doi.org/10.1007/s00410-020-01715-y.

Tait, S.R., Wörner, G., Van Den Bogaard, P., Schmincke, H.-U., 1989. Cumulate nodules as evidence for convective fractionation in a phonolite magma chamber. J. Volcanol. Geotherm. Res. 37, 21–37.

Textor, C., Sachs, P.M., Graf, H.-F., Hansteen, T.H., 2003. The 12 900 years BP Laacher See eruption: estimation of volatile yields and simulation of their fate in the plume. Geol. Soc. (Lond.) Spec. Publ. 213, 307. https://doi.org/10.1144/GSL.SP.2003.213.01.19.

Tomlinson, E.L., Smith, V.C., Menzies, M.A., 2020. Chemical zoning and open system processes in the Laacher See magmatic system. Contrib. Mineral. Petrol. 175, 19.

Truby, J.M., 2016. Rheology, eruption, and flow of three-phase magma (PhD), Durham University.

Webster, J.D., 1992. Fluid-melt interactions involving Cl-rich granites: experimental study from 2 to 8 kbar. Geochim. Cosmochim. Acta 56, 659–678.

Webster, J.D., Tappen, C.M., Mandeville, C.W., 2009. Partitioning behavior of chlorine and fluorine in the system apatite–melt–fluid, II: felsic silicate systems at 200 MPa. Geochim. Cosmochim. Acta 73, 559–581. https://doi.org/10.1016/j.gca.2008.10.034.

Wörner, G., Beusen, J.-M., Duchateau, N., Gijbels, R., Schmincke, H.-U., 1983. Trace element abundances and mineral/melt distribution coefficients in phonolites from the Laacher See Volcano (Germany). Contributions to. Mineral. Petrol. 84, 152–173.

Wörner, G., Schmincke, H.-U., 1984a. Petrogenesis of the zoned Laacher See tephra. J. Petrol. 25, 836–851.

Wörner, G., Schmincke, H.-U., 1984b. Mineralogical and chemical zonation of the Laacher See tephra sequence (East Eifel, W. Germany). J. Petrol. 25, 805–835.

Wörner, G., Wright, T.L., 1984. Evidence for magma mixing within the Laacher See magma chamber (East Eifel, Germany). J. Volcanol. Geotherm. Res. 22, 301–327.

Chevychelov, V.Yu., Botcharnikov, R.E., Holtz, F., 2008. Partitioning of Cl and F between fluid and hydrous phonolitic melt of Mt. Vesuvius at ~850–1000 °C and 200 MPa. Chem. Geol. 256, 172–184. https://doi.org/10.1016/j.chemgeo.2008.06.025.

Zhang, Y., 1999. H_2O in rhyolitic glasses and melts: measurement, speciation, solubility, and diffusion. Rev. Geophys. 37, 493–516.